Supplementary References

1. Bi D, Nishimura J, Niiro N, Hirano K, Kanaide H. Contractile properties of the cultured vascular smooth muscle cells: the crucial role played by RhoA in the regulation of contractility. *Circ Res.* 2005;96:890-897.
2. Hamilton BA, Frankel WN, Kerrebrock AW, Hawkins TL, FitzHugh W, Kusumi K, Russell LB, Mueller KL, van Berkel V, Birren BW, Kruglyak L, Lander ES. Disruption of the nuclear hormone receptor RORα in staggerer mice. *Nature.* 1996;379:736-739.
3. Qiu CH, Shimokawa N, Iwasaki T, Parhar IS, Koibuchi N. Alteration of cerebellar neurotropin messenger ribonucleic acids and the lack of thyroid hormone receptor augmentation by staggerer-type retinoic acid receptor-related orphan receptor-α mutation. *Endocrinology.* 2007;148:1745-1753.
4. Kikkawa Y, Kameda K, Hirano M, Sasaki T, Hirano K. Impaired feedback regulation of the receptor activity and the myofilament Ca^{2+} sensitivity contributes to increased vascular reactiveness after subarachnoid hemorrhage. *J Cereb Blood Flow Metab.* 2010;30:1637-1650.
5. Hirano M, Kanaide H, Hirano K. Rac1-dependent transcriptional up-regulation of $p27^{Kip1}$ by homophilic cell-cell contact in vascular endothelial cells. *Biochim Biophys Acta.* 2007;1773:1500-1510.
6. Maeda Y, Hirano K, Kai Y, Hirano M, Suzuki SO, Sasaki T, Kanaide H. Up-regulation of proteinase-activated receptor 1 and increased contractile responses to thrombin after subarachnoid haemorrhage. *Br J Pharmacol.* 2007;152:1131-1139.
7. Harding HP, Lazar MA. The orphan receptor Rev-ErbA α activates transcription via a novel response element. *Mol Cell Biol.* 1993;13:3113-3121.

Hypertension Research (2012), 1–8

www.nature.com/hr

ORIGINAL ARTICLE

Mineralocorticoid receptors/epithelial Na^+ channels in the choroid plexus are involved in hypertensive mechanisms in stroke-prone spontaneously hypertensive rats

Masatsugu Nakano[1], Yoshitaka Hirooka[2], Ryuichi Matsukawa[1], Koji Ito[1] and Kenji Sunagawa[1]

Increase in cerebrospinal fluid (CSF) Na^+ concentration ($[Na^+]$) precedes hypertension and is a key step in the development of salt-induced hypertension. In the choroid plexus (CP), epithelial Na^+ channels (ENaCs) have an important role in Na^+ transport from the blood into the CSF. However, it remains unknown whether the mineralocorticoid receptors (MR)/ENaCs pathway in the CP of stroke-prone spontaneously hypertensive rats (SHRSP) is involved in neural mechanisms of hypertension. Therefore, we examined the role of the MR/ENaCs pathway in the CP in the development of hypertension in SHRSP associated with an increase in CSF $[Na^+]$. As a marker of MR activation, serum/glucocorticoid-inducible kinase 1 (Sgk1) expression levels in the CP were measured and found to be greater in SHRSP than in Wistar–Kyoto (WKY) rats. CSF $[Na^+]$ levels were also higher in SHRSP than in WKY rats. In SHRSP, high-salt intake (8%) increased blood pressure and urinary norepinephrine excretion compared with those in animals fed a regular salt diet (0.5%) for 2 weeks. Furthermore, the expression levels of MR, Sgk1 and ENaCs in the CP and the increase in CSF $[Na^+]$ were greater in SHRSP fed a high-salt diet than in those fed a regular salt diet. These alterations were attenuated by intracerebroventricular infusion of eplerenone (10 $\mu g\,kg^{-1}$ per day), except for α-ENaC and β-ENaC. We conclude that activation of the MR/ENaCs pathway in the CP contributes to hypertension via an increase in CSF $[Na^+]$, thereby exaggerating salt-induced hypertension with sympathetic hyperactivation in SHRSP.
Hypertension Research advance online publication, 25 October 2012; doi:10.1038/hr.2012.174

Keywords: brain; choroid plexus; epithelial sodium channels; mineralocorticoid receptor; sympathetic nervous system

INTRODUCTION

Hypertension is a major risk factor for cardiovascular diseases.[1] The percentages of essential hypertension patients who are salt sensitive have varied widely among study cohorts, ranging between 30 and 70%.[2] The appropriate therapeutic target of salt-induced hypertension has been determined to be volume overload, so that sodium restriction and diuretics are beneficial for salt-induced hypertension.[3,4] Abnormal sympathetic hyperactivity has also been detected in patients with salt-induced hypertension.[5,6] Thus, in addition to the role of kidney, the central nervous system has an important role in salt-induced hypertension.[6,7]

An increase in cerebrospinal fluid (CSF) Na^+ concentration ($[Na^+]$) is responsible for activation of the central sympathetic outflow.[8,9] High-salt intake elicits an increase in CSF $[Na^+]$ and causes sympathetic hyperactivity and hypertension in salt-sensitive model rats, such as Dahl S rats.[7,10] It has also been demonstrated that an increase in CSF $[Na^+]$ causes central aldosterone production, mineralocorticoid receptors (MR) activation and renin–angiotensin system (RAS) activation, thereby leading to sympathetic hyperactivity.[11] On the other hand, high-salt intake does not affect CSF $[Na^+]$, blood pressure (BP) or heart rate (HR) in normotensive model rats.[8] However, intracerebroventricular (ICV) infusion of Na^+-rich artificial CSF elicits MR activation in the hypothalamus, leading to increase in BP through sympathoexcitation in both salt-sensitive model rats and normotensive model rats, although the extent of sympathoexcitation is greater in salt-sensitive rats than in normotensive rats.[12,13] These observations suggest that an increase in Na^+ in the brain elicits sympathoexcitation irrespective of the presence/absence of salt-sensitive hypertension. However, it is possible that the mechanisms of Na^+ transport into the brain might be different between normotensive and hypertensive models.

The epithelium of the choroid plexus (CP) is the major site for production of CSF, which is later absorbed by arachnoid granulations.[14,15] Enhanced Na^+ uptake from the plasma to the CSF might

[1]Department of Cardiovascular Medicine, Kyushu University Graduate School of Medical Sciences, Fukuoka, Japan and [2]Department of Advanced Cardiovascular Regulation and Therapeutics, Kyushu University Graduate School of Medical Sciences, Fukuoka, Japan
Correspondence: Dr Y Hirooka, Department of Advanced Cardiovascular Regulation and Therapeutics, Kyushu University Graduate School of Medical Sciences, 3-1-1 Maidashi, Higashi-ku, Fukuoka 812-8582, Japan.
E-mail: hyoshi@cardiol.med.kyushu-u.ac.jp
Received 7 June 2012; revised 26 August 2012; accepted 29 August 2012

therefore be an important step in the initiation of salt-induced hypertension in salt-sensitive hypertensive models. Epithelial Na^+ channels (ENaCs) in the choroidal epithelia actively support Na^+ influx from the plasma and, in general, Na^+ levels in the CSF are higher than those in the plasma.[16] The ENaCs form a heteromultimeric channel that is composed of three homologous α-, β- and γ-subunits.[17] Both MR activation itself and the resulting MR-induced activation of serum/glucocorticoid-inducible kinase 1 (Sgk1) augment the expression of ENaCs in the kidney.[18] Sgk1 is a key downstream effector of MR signaling in the kidneys, inducing the early and late responses through regulation of the epithelial sodium channel activity, trafficking, and transcription.[19–21] The Sgk1 expression level also reflects MR activation, and used for this purpose because MR expression itself is not equal to MR activation.[22] However, the mechanism by which the MR/ENaCs pathway in the CP contributes to an increase in CSF $[Na^+]$ and sympathoexcitation, and leads to hypertension in hypertensive model rats, remains unclear.

Stroke-prone spontaneously hypertensive rats (SHRSP) serve as an experimental model of salt-loading-accelerated hypertension.[23,24] We hypothesized that an increase in CSF $[Na^+]$ might be involved in the development of hypertension in the absence of sodium loading, or might worsen hypertension in the presence of sodium loading in SHRSP via irregularities in the MR/ENaCs pathway in the CP. Therefore, the aim of the present study was to determine whether the MR/ENaCs pathway in the CP was altered in SHRSP and, if so, to examine whether this alteration was involved in abnormal sympathetic hyperactivity with or without sodium loading in SHRSP. For this purpose, we compared the expressions of MR, Sgk1 and ENaCs in the CP without sodium loading between SHRSP and Wistar–Kyoto (WKY) rats. Furthermore, we investigated these expressions in SHRSP fed a high-salt diet. Finally, we investigated the effect of ICV infusion of an MR blocker concomitant with high-salt loading on sympathetic activity and CSF $[Na^+]$.

METHODS

Animals

This study was reviewed and approved by the Committee on Ethics of Animal Experiments, Kyushu University Graduate School of Medical Sciences, and conducted according to the Guidelines for Animal Experiments of Kyushu University. Male WKY rats and SHRSP (260–330 g; 12–14 weeks old) were obtained from SLC Japan (Hamamatsu, Japan). They were housed in temperature- (23 ± 2°C) and light-controlled animal quarters and were provided with rat chow *ad libitum*.

Western blot analysis

Rats were killed with an overdose of sodium pentobarbital and the tissues of CP were obtained. The tissues were removed and homogenized in a lysis buffer. The protein concentration was determined using a bicinchonic acid protein assay kit (Pierce Chemical, Rockford, IL, USA). A 15-μg aliquot of protein from each sample was separated on a polyacrylamide gel with 10% sodium dodecyl sulfate. The proteins were then transferred onto polyvinylidene difluoride membranes (Immobilon-P membranes; Millipore, Billerica, MA, USA), and the membranes were incubated with rabbit immunoglobulin G (IgG) polyclonal antibody to MR (1:1000; Santa Cruz Biotechnology, Santa Cruz, CA, USA), with goat IgG polyclonal antibody to α-ENaC, rabbit polyclonal antibody to β-ENaC or rabbit polyclonal antibody to γ-ENaC (1:1000; Santa Cruz Biotechnology), or with rabbit IgG polyclonal antibody to Sgk1 (1:1000; Abcam, Cambridge, UK). Next, the membranes were incubated with horseradish peroxidase-conjugated horse anti-rabbit or anti-goat IgG antibody (1:10 000). Glyceraldehyde 3-phosphate dehydrogenase (GAPDH) was used as an internal control for the brain tissues. Immunoreactivity was detected by enhanced chemiluminescence autoradiography (ECL Western blotting detection kit; Amersham Pharmacia Biotech, Uppsala, Sweden), and the film was analyzed using the public domain software NIH Image (developed at the US National Institutes of Health and available on the Internet at http://rsb.info.nih.gov/nih-image/).

Measurement of CSF $[Na^+]$ and plasma $[Na^+]$

The CSF was collected via puncture of the cisterna magna. CSF $[Na^+]$ was measured using an ion-selective electrode (model MI-425; Microelectrodes, Bedford, NH, USA). Plasma $[Na^+]$ was measured at SRL (Tokyo, Japan).

Intracarotid artery (ICA) infusion of NaCl in acute experiments

Rats were anesthetized with pentobarbital (50 mg kg^{-1} i.p. followed by 20 mg kg^{-1} h^{-1} i.v.) and artificially ventilated. A catheter (polyethylene (PE)-50 tubing) was inserted into the left internal carotid artery and NaCl (0.5 M, 1 M, 10 s for each injection, total infusion volume; 300 μl) was administered. A catheter was implanted into the left ICA and advanced 1.0–1.3 cm beyond the carotid sinus to avoid activation of arterial baroreceptors. Another catheter was then inserted into the left femoral artery to measure BP and HR. A pair of stainless steel bipolar electrodes was placed beneath the renal nerve to record multifiber renal sympathetic nerve activity.[25,26] All signals were recorded on a computer using a PowerLab system (AD Instruments, Colorado Springs, CO, USA). The signal from the electrodes was amplified, passed through a band pass filter, and then rectified and integrated (resetting every 0.1 s).

Measurements of BP and sympathetic activity in chronic experiments

Systolic BP of conscious animals was measured using tail-cuff plethysmography (BP-98 A; Softron, Tokyo, Japan). Sympathetic activity was evaluated by measuring 24-h urinary norepinephrine excretion using high-performance liquid chromatography before and at day 14. Urinary norepinephrine excretion was calculated as described previously.[27]

ICV infusion of eplerenone

Under sodium pentobarbital anesthesia (50 mg kg^{-1} i.p.) rats were placed in a stereotaxic frame. The skin overlying the midline of the skull was incised and a small hole was made with a dental drill at the following coordinates: 0.8 mm posterior and 1.5 mm lateral relative to bregma. The infusion cannula from an Alzet brain infusion kit 2 (DURECT Corporation, Cupertino, CA, USA) connected to an osmotic pump (model 2002; Alzet) was lowered 3.5 mm below the skull surface and fixed to the skull surface with tissue adhesive. The osmotic mini pump was inserted subcutaneously in the back. The ICV infusion of artificial CSF + vehicle (1% DMSO) or artificial CSF + eplerenone (10 μg kg^{-1}per day in vehicle) (kindly provided by Pfizer Pharmaceutical Company, New York, NY, USA) for 2 weeks was performed in conjunction with feeding of a high-salt diet, and the infusion and diet were started simultaneously.

Experimental protocols

Protocol 1: Experiments with rats without salt loading. (1) Western blot analysis of MR, Sgk1 and ENaCs in the CP of SHRSP and WKY rats; (2) evaluations of CSF $[Na^+]$ and plasma $[Na^+]$ in SHRSP and WKY rats; (3) acute bolus ICA injection of NaCl (0.5 M, 1 M, 300 μl per 10 s) in SHRSP and WKY rats. The rats were fed a regular diet.

Protocol 2: Experiments with rats fed a high-salt diet. SHRSP and WKY rats were divided randomly into two groups: rats fed a high-salt (8% NaCl) diet for 2 weeks and rats fed a regular (0.5% NaCl) diet for 2 weeks. Then, the following protocols were performed. (1) Western blot analysis of MR, Sgk1 and ENaCs in the CP of SHRSP and WKY rats fed a high-salt or regular diet; (2) evaluations of CSF $[Na^+]$ in SHRSP and WKY rats fed a high-salt diet.

Protocol 3: Experiments with SHRSP fed a high-salt diet with eplerenone. ICV infusion of artificial CSF or eplerenone for 2 weeks in SHRSP fed a high-salt diet. Then, the following protocols were performed. (1) Measurement of BP and HR using the tail-cuff method; (2) western blot analysis of MR, Sgk1 and

ENaCs in the CP; (3) Evaluations of CSF [Na^+] and urinary norepinephrine in SHRSP.

Statistical analysis

All values are expressed as the means ± s.e.m. Intergroup differences in the mean arterial pressure (MAP) and HR values obtained using the PowerLab and tail-cuff method were compared using two-way analysis of variance. In the analysis of variance, comparisons between any two mean values were performed using Bonferroni's correction for multiple comparisons. The MR, Sgk1 and ENaCs protein expression values (western blot analysis), and the CSF [Na^+] and plasma [Na^+] values were compared using an unpaired *t*-test. Values of $P<0.05$ were considered statistically significant.

RESULTS

Baseline MR, Sgk1 and ENaCs expressions in the CP of SHRSP and WKY rats fed a regular diet

MR expression in SHRSP did not differ from that in WKY rats, while Sgk1 expression was significantly greater in SHRSP (Figure 1a). The expressions of α-ENaC, β-ENaC and γ-ENaC were also significantly higher in SHRSP than in WKY rats (Figure 1b).

Baseline plasma [Na^+] and CSF [Na^+] of SHRSP and WKY rats fed a regular diet

Plasma [Na^+] levels did not differ between WKY rats and SHRSP (WKY, 145.4 ± 0.8 mM; SHRSP, 145.1 ± 0.8 mM; $n=7$ for each), but the level of CSF [Na^+] was greater in SHRSP (WKY, 151.9 ± 0.4 mM; SHRSP, 155.5 ± 0.3 mM, $n=6$ for each; Figure 1c).

Effect of ICA NaCl infusion on MAP, HR and renal sympathetic nerve activity in SHRSP and WKY rats

ICA hypertonic NaCl (0.5 M, 1.0 M) infusions increased MAP in both WKY rats and SHRSP dose-dependently. However, the degrees of increase in MAP were greater in SHRSP than in WKY rats (% change of ΔMAP: WKY *vs.* SHRSP, 3.0 ± 2.3% *vs.* 14.4 ± 2.5%, $P<0.05$ (0.5 M); 7.5 ± 4.3% *vs.* 35.1 ± 5.5%, $P<0.005$ (1.0 M); $n=5$ for each; Figure 2). The duration of the responses lasted longer in SHRSP than WKY rats (WKY *vs.* SHRSP, 2.3 ± 0.4 *vs.* 5.9 ± 0.6 min, $P<0.01$ (0.5 M); 4.3 ± 0.5 *vs.* 14.3 ± 1.5 min, $P<0.01$ (1.0 M); $n=5$ for each). Peak responses of renal sympathetic nerve activity (% baseline) to NaCl were also greater in SHRSP than in WKY rats (% baseline: WKY *vs.* SHRSP, 6.5 ± 3.7% *vs.* 20.3 ± 1.1%, $P<0.01$ (0.5 M); 13.8 ± 1.7% *vs.* 30.0 ± 5.3%, $P<0.05$ (1.0 M); $n=4$-5 for each; Figure 2).

Effects of high-salt diet on systolic BP and CSF [Na^+] in SHRSP and WKY rats

Systolic BP and HR of in SHRSP groups were significantly higher than those of WKY rats throughout the study (Table 1). SHRSP fed a high-salt diet exhibited a significantly higher systolic BP and HR than SHRSP fed a regular diet, starting at 12 weeks of age ($P<0.05$). Systolic BP also slightly increased in SHRSP fed a regular diet ($P<0.05$). Systolic BP and HR values for 2 weeks are shown in

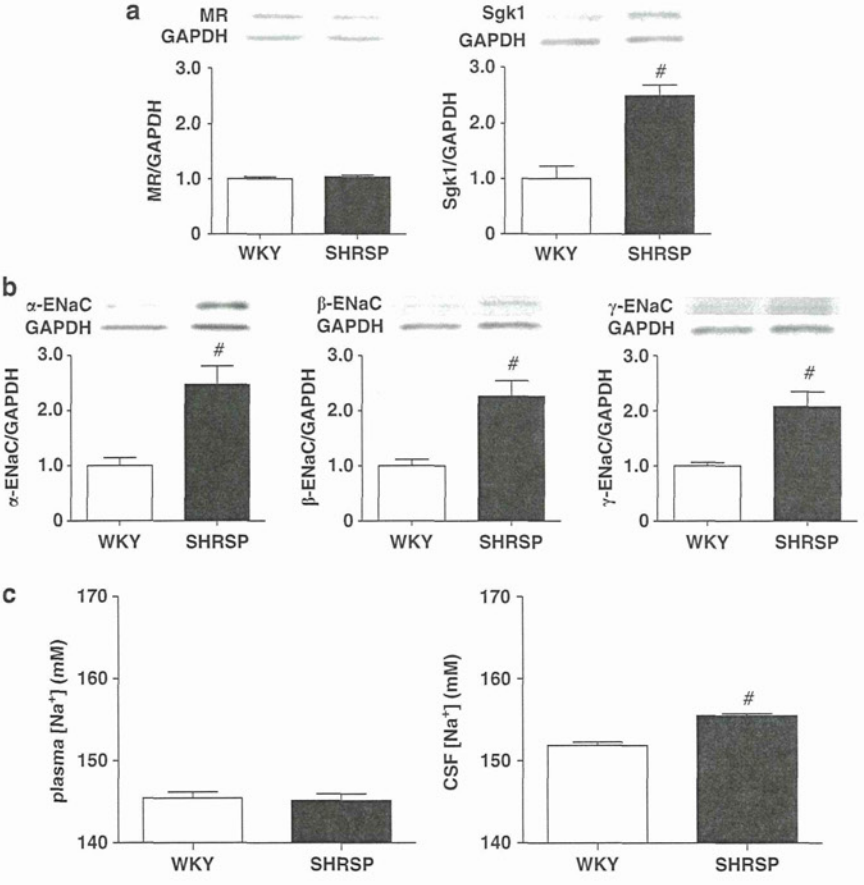

Figure 1 Western blot analysis demonstrating the expression levels of (**a**) the MR and Sgk1, and (**b**) α-, β- and γ-ENaCs in the CP of 12-week-old WKY and SHRSP rats. The densitometric average was normalized to the values obtained from the analysis of glyceraldehyde-3-phosphatase dehydrogenase (GAPDH) as an internal control. Expressions are shown relative to those seen in WKY rats, which are assigned a value of 1. Values are expressed as the mean ± s.e.m. $^{\#}P<0.01$; $n=4$–5. (**c**) Plasma [Na^+] and CSF [Na^+] levels in WKY rats and SHRSP. $^{\#}P<0.01$; $n=6$–7.

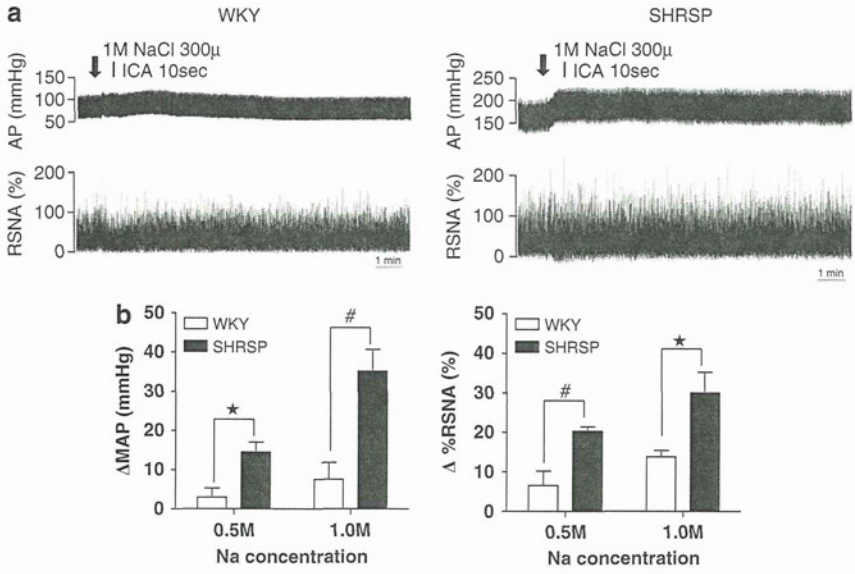

Figure 2 The responses of arterial pressure (AP) and renal sympathetic nerve activity (RSNA) to ICA NaCl (0.5 M, 1 M) infusions. (**a**) Raw data of the changes in AP and RSNA after ICA NaCl (1 M) infusions in WKY rats and SHRSP. (**b**) Group data of the changes in MAP and RSNA in response to ICA NaCl (0.5 M, 1 M) infusions. Values are expressed as the mean ± s.e.m. $^{*}P<0.05$, $^{\#}P<0.01$; $n=4$–5.

Table 1 BP and HR with a regular diet or a high-salt diet in WKY and SHRSP

	Systolic BP (mm Hg)				*HR (b.p.m.)*			
Weeks	*HS-SP*	*RS-SP*	*HS-W*	*RS-W*	*HS-SP*	*RS-SP*	*HS-W*	*RS-W*
12	219 ± 3$^{\#}$	216 ± 2$^{\#}$	134 ± 2	135 ± 2	374 ± 2$^{\#}$	373 ± 3$^{\#}$	352 ± 2	349 ± 4
13	235 ± 4$^{\#*}$	223 ± 2$^{\#}$	137 ± 2	134 ± 2	385 ± 4$^{\#*}$	373 ± 4$^{\#}$	359 ± 5	356 ± 3
14	253 ± 2$^{\#*}$	227 ± 2$^{\#}$	138 ± 2	136 ± 1	390 ± 2$^{\#*}$	370 ± 4$^{\#}$	358 ± 3	351 ± 5

Abbreviations: BP, blood pressure; HR, heart rate; HS-SP, high-salt diet SHRSP rats; HS-W, high-salt diet WKY rats; RS-SP, regular diet SHRSP rats; RS-W, regular diet WKY rats; SHRSP, spontaneously hypertensive stroke-prone rats; WKY, Wistar–Kyoto rats.
Values are given as mean ± s.e.m. $^{*}P<0.05$, HS-SP *vs.* RS-SP; $^{\#}P<0.05$, SHRSP *vs.* WKY. $n=7$.

Table 1. CSF [Na^+] in SHRSP also started to increase from day 4 (152.3 ± 0.8 *vs.*158.6 ± 0.4 mM, $P<0.05$). At day 14, CSF [Na^+] in SHRSP fed a high-salt diet was significantly greater than in WKY fed a high-salt diet (152.4 ± 0.4 *vs.*161.1 ± 0.4 mM; Figure 3a). In contrast, in WKY rats, there were no significant changes in systolic BP and CSF [Na^+] during the observation (Figure 3a and Table 1).

Expression of MR, Sgk1 and ENaCs in the CP in SHRSP and WKY rats fed a high-salt diet

The expressions of MR, Sgk1 and ENaCs were significantly greater in SHRSP fed a high-salt diet than in those fed a regular diet (Figure 3b). The expressions of MR, Sgk1 and ENaCs were similar between WKY rats fed a high-salt diet and those fed a regular diet (Figure 3c).

Effects of eplerenone on systolic BP, sympathetic activity, CSF [Na^+], and expression levels of MR, Sgk1 and ENaCs in SHRSP fed a high-salt diet

ICV infusion of eplerenone attenuated the increases in urinary norepinephrine and systolic BP in SHRSP fed a high-salt diet (Figures 4a and b). ICV infusion of eplerenone attenuated the increase in CSF [Na^+] in SHRSP fed a high-salt diet (157.8 ± 0.92 *vs.* 161.0 ± 0.73 mM; Figure 4c). ICV infusion of eplerenone did not attenuate the enhanced expressions of MR, α-ENaC and β-ENaC, but did attenuate Sgk1 and γ-ENaC expression (Figures 5a and b).

DISCUSSION

The present study demonstrated that the MR/ENaCs pathway in the CP of SHRSP was activated before salt loading, leading to an increase in the CSF [Na^+] and eliciting sympathetic hyperactivity. Salt loading then elicited further activation of this pathway in the CP and an additional increase in CSF [Na^+], thereby causing further sympathetic hyperactivity and BP elevation.

We first investigated the alterations of the Na^+ transport system in the CP of SHRSP and found that the expressions of all subunit types of ENaCs were greater in SHRSP than in WKY rats. These data suggest that the function of the Na^+ transport system in the CP was enhanced in SHRSP. In fact, the plasma [Na^+] level was similar between SHRSP and WKY rats, but the CSF [Na^+] level was greater in SHRSP than in WKY rats. Taken together, these data suggest that activation of ENaCs in the CP elicited increase in CSF [Na^+] in SHRSP.

We considered that these alterations occurring in SHRSP may contribute to the development of hypertension. Thus, we investigated whether activated ENaCs in the CP contribute to the development of hypertension with sympathetic hyperactivity. ICA infusions of hypertonic NaCl solutions increased renal sympathetic nerve activity and AP and the degrees of these changes were greater in SHRSP than in WKY rats. It has been reported that increases in the amount of plasma [Na^+] perfusing the forebrain evoke a prompt increase

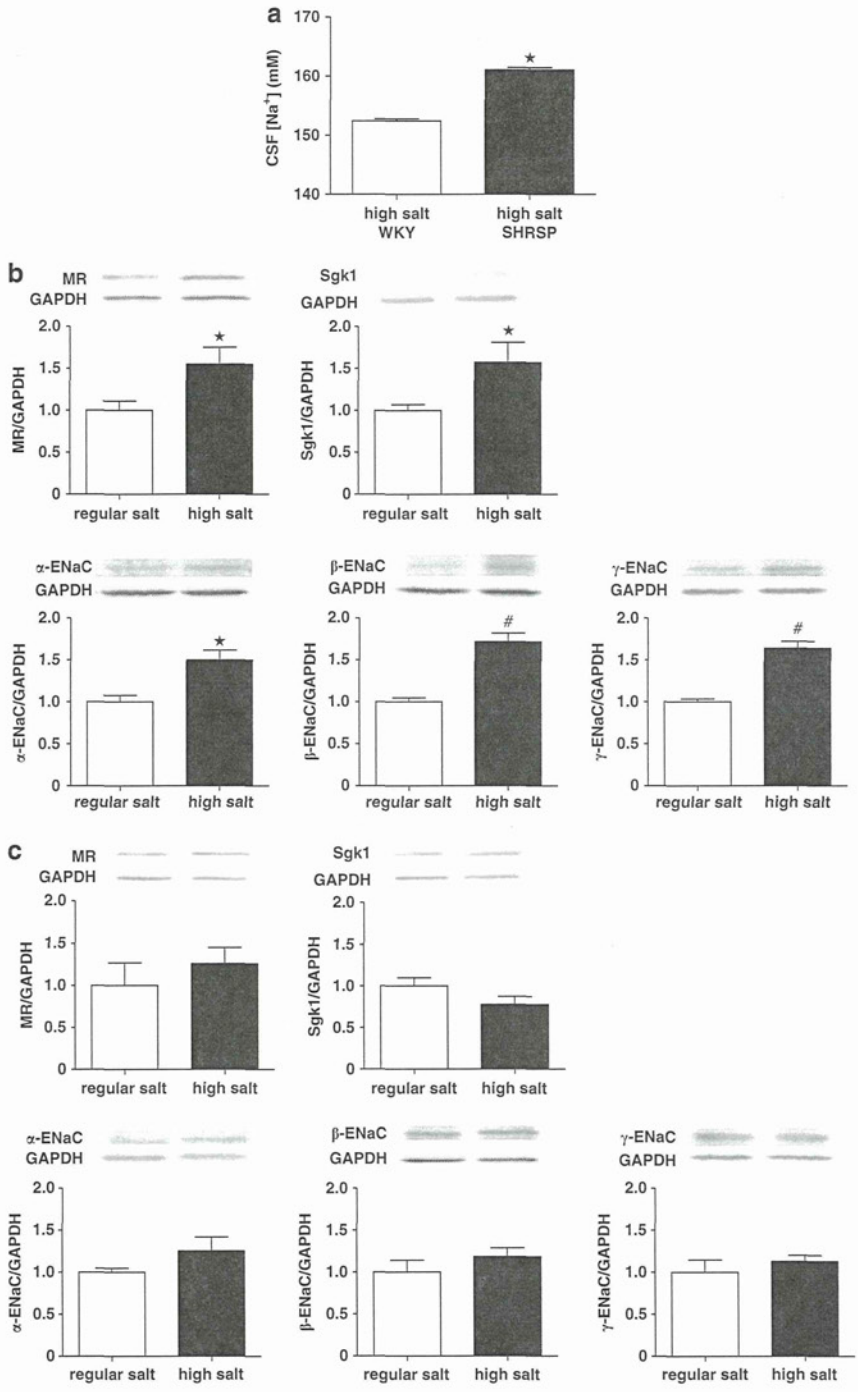

Figure 3 (**a**) CSF [Na^+] in WKY rats and SHRSP by feeding with a high-salt diet at day 14. Values are expressed as the mean ± s.e.m. $^*P<0.05$; $n=7$ for each. (**b**) Western blot analysis demonstrating MR, Sgk1, α-, β- and γ- ENaC expression in the CP in SHRSP fed a high-salt or regular diet. The densitometric average is normalized to the values obtained from the analysis of GAPDH as an internal control. Expressions are shown relative to those in SHRSP fed a regular diet, which are assigned a value of 1. (**c**) Western blot analysis demonstrating MR, Sgk1, α-, β- and γ- ENaC expression in the CP in WKY rats fed a high-salt or regular diet. The densitometric average is normalized to the values obtained from the analysis of GAPDH as an internal control. Expressions are shown relative to those in WKY rats fed a regular diet, which are assigned a value of 1. Values are expressed as the mean ± s.e.m. $^*P<0.05$, $^{\#}P<0.01$; $n=4$–6.

of sympathetic nerve activity.[28,29] An increase in CSF [Na^+] may excite Na^+-sensitive neurons in the circumventricular organs, such as the subfornical organ.[30] This increased neuronal activity could be relayed to the paraventricular nucleus of the hypothalamus or rostral ventrolateral medulla, thereby increasing sympathetic nerve activity and BP.[31–33] Furthermore, an increase in CSF [Na^+] would increase the level of hypothalamic tissue [Na^+][34] and could thereby enhance the firing activity of Na^+-sensitive neurons in the paraventricular nucleus.[35] We also need to consider the possibility that circumventricular organs could sense hyperosmolality after ICA infusions of hypertonic NaCl solutions thereby activates sympathetic activity, although there is a clear difference between SHRSP and WKY rats.[36] In addition, the duration of the responses lasted longer in SHRSP than WKY rats. We were not able to measure CSF [Na^+]

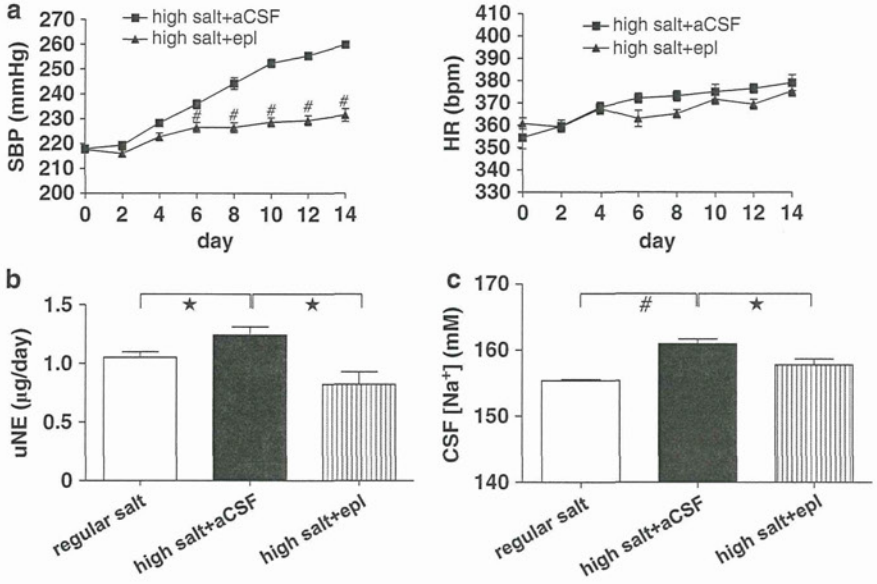

Figure 4 Effects of ICV infusion of artificial CSF (aCSF) (high salt + aCSF) *vs.* eplerenone at 10 μg kg^{-1} per day (high salt + epl) in CP of SHRSP on systolic BP (SBP), heart rate (HR), sympathetic nerve activity and CSF [Na^+] induced by high-salt intake. (**a**) Changes in resting SBP and HR response to ICV infusion of aCSF or eplerenone in rats fed a high-salt diet. $^{\#}P<0.01$; $n=6$ for each. (**b**) Group data for urinary norepinephrine excretion in SHRSP given a regular diet, a high-salt diet plus ICV infusion of aCSF (high salt + aCSF) or a high-salt diet plus eplerenone (high salt + epl). $^{*}P<0.05$; $n=5$–6. (**c**) Group data for CSF [Na^+] in SHRSP given a regular diet (regular), a high-salt diet plus ICV infusion of aCSF (high salt + aCSF) or a high-salt diet plus eplerenone (high salt + epl). $^{*}P<0.05$, $^{\#}P<0.01$; $n=10$ for each.

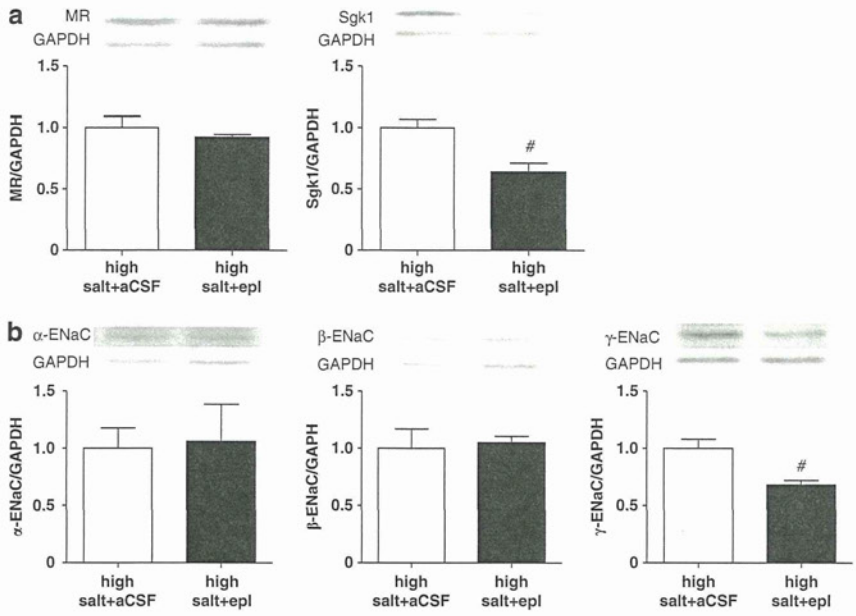

Figure 5 Effects of ICV infusion of artificial CSF (aCSF) (high salt + aCSF) *vs.* eplerenone at 10 μg kg^{-1} per day (high salt + epl) in the CP of SHRSP. Western blot analysis demonstrating the expression of (**a**) MR, Sgk1, or (**b**) α-, β- and γ- ENaC in the CP in high salt + aCSF *vs.* high salt + epl. The densitometric average was normalized to the values obtained from the analysis of glyceraldehyde-3-phosphatase dehydrogenase (GAPDH) as an internal control. Expressions are shown relative to those seen in the high salt + aCSF group, which were assigned a value of 1. Values are expressed as the mean ± s.e.m. $^{\#}P<0.01$; $n=4$–6.

before and after ICA infusion because of technical difficulties. However, these data indirectly suggest that Na^+ uptake into the CSF is enhanced and this contributes to hypertension with sympathoexcitation in SHRSP without salt loading.

In salt-sensitive model rats, high-salt intake causes an increase in CSF [Na^+] and leads to sympathetic hyperactivity and hypertension.[7,37,38] SHRSP are also known as a salt-induced hypertension model.[24] A high-salt diet elicited hypertension with sympathetic hyperactivity in SHRSP as previously described.[24,39] We found that the expressions of all subtypes of ENaCs in the CP and CSF [Na^+] were increased in SHRSP fed a high-salt diet concomitant with changes in MAP. These data suggest that activated ENaCs in the

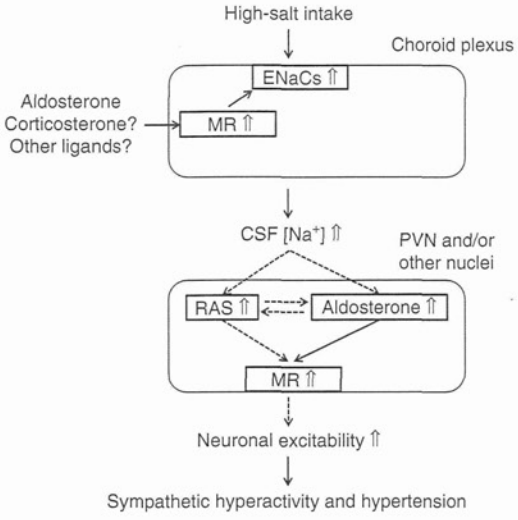

Figure 6 The possible cascade that Na^+ transport mechanisms in the central nervous system contributing to sympathetic hyperactivity and hypertension in SHRSP on high-salt intake. In SHRSP on high-salt intake, Na^+ transport into CSF is enhanced and CSF [Na^+] is increased. Activation of MR/ENaCs pathway in the choroid plexus is involved in Na^+ transport from the blood into the CSF in SHRSP. The increased CSF [Na^+] increased the neuronal activity in the PVN or other autonomic nuclei, thereby increasing the central sympathetic outflow. This, in turn, leads to sympathetic hyperactivity and hypertension. The broken lines indicate hypothetical mechanisms suggested by other investigators. RAS indicates renin–angiotensin system.

CP of SHRSP accelerated the increase in CSF [Na^+], and this increase further enhanced the levels of ENaCs, leading to sympathetic hyperactivity (Figure 6).

It has been shown that aldosterone binds to MR and increases expression and activity of ENaCs in the distal nephron of the kidney, resulting in enhanced Na^+ and water reabsorption, and presumably thereby elevated BP.[18] We recently reported that activation of the MR/ENaCs pathway is considered to be an initial step in the acquisition of Na^+ sensitivity in the brain in a pressure overload model.[40] In fact, Western blotting in the present study revealed that the expression of Sgk1 was increased in SHRSP compared with WKY rats before salt loading, although the expression levels of MR did not differ between SHRSP and WKY rats. Moreover, expressions of MR and ENaCs in the CP were increased by salt loading in SHRSP. Taken together with the alterations of ENaCs, our findings suggest that MR and ENaCs in the CP are altered in parallel with or without salt loading in SHRSP. We also found that ICV infusion of an MR blocker attenuated BP elevation and increase in CSF [Na^+] induced by chronic salt loading in SHRSP. Furthermore, the MR blocker inhibited the increase in Sgk1 expressions and γ-ENaC in the CP of SHRSP. However, we do not have a clear explanation why only γ-ENaC was smaller for eplerenon treated SHRSP on high-salt diet at the present time. There may be subunit-type-specific regulation of ENaC.[40] These findings suggest that MR regulates Na^+ transport into the CSF by regulating the expressions of ENaCs in the CP of SHRSP, although we did not find the increased expression levels of α-ENaC and β-ENaC.

In consistent with the results of a previous study, SHRSP have significantly higher plasma aldosterone levels compared with WKY rats, indicating upregulation of the aldosterone system in SHRSP.[24] If the aldosterone is the ligand of MR in the CP of SHRSP, MR is activated in SHRSP. In salt-sensitive model rats, high-salt intake produces aldosterone locally in the hypothalamus.[11,41] Another possibility is that locally produced aldosterone may affect MR activation in the CP via CSF.[41,42] In the absence of 11β-hydroxysteroid dehydrogenase type 2 in the CP, corticosterone is also a ligand for MR.[43] On the other hand, Rac1 enhances MR independent of aldosterone in the kidney.[44] We did not address precise mechanisms how MR in the CP was activated in SHRSP in the present study. Nevertheless, our findings suggest that MR activation has an important role for the increase in central sympathetic outflow in SHRSP. Further studies are necessary to clarify this important question.

The present study has some additional limitations. First, ENaCs exist on both the apical and basolateral side of the CP.[34,45] We did not examine the distribution of ENaCs in the CP in the present study because of the technical difficulty. Second, ICV infusion of an MR blocker may act on the nuclei other than those in the CP.[46,47] Third, Na^+-K^+-ATPase activity in the CP is also dependent on CSF [Na^+] in Dahl salt-sensitive rats.[48] MR regulates the transcription of Na^+-K^+-ATPase.[49] Both ENaCs and Na^+-K^+-ATPase regulate Na^+ transport in the CP. Further studies will be needed to clarify whether Na^+-K^+-ATPase alterations are involved in our observations in the present study.

In conclusion, our findings suggest that the MR/ENaCs pathway in the CP of SHRSP is activated before salt loading, leading to an increased CSF [Na^+] and eliciting sympathetic hyperactivity. Second suggestion is that salt loading elicited further activation of this pathway in the CP and additional enhancement of the CSF [Na^+] levels, leading to further sympathetic hyperactivity.

CONFLICT OF INTEREST

The authors declare no conflict of interest.

ACKNOWLEDGEMENTS

We express our sincere thanks to Naomi Shirouzu for help with the western blot analysis. This study was supported by the Grants-in-Aid for Scientific Research from the Japan Society for Promotion of Science (23220013, 24390198) and, in part, a Grant from the Salt Science Research Foundation (1233).

1 Rosamond W, Flegal K, Friday G, Furie K, Go A, Greenlund K, Haase N, Ho M, Howard V, Kissela B, Kittner S, Lloyd-Jones D, McDermott M, Meigs J, Moy C, Nichol G, O'Donnell CJ, Roger V, Rumsfeld J, Sorlie P, Steinberger J, Thom T, Wasserthiel-Smoller S, Hong Y. American Heart Association Statistics Committee and Stroke Statistics Subcommittee. Heart disease and stroke statistics–2007 update: A report from the american heart association statistics committee and stroke statistics subcommittee. *Circulation* 2007; **115**: e69–e171.
2 Rassler B. The renin-angiotensin system in the development of salt-sensitive hypertension in animal models and humans. *Pharmaceuticals* 2010; **3**: 940–960.
3 Kawano Y. Diurnal blood pressure variation and related behavioral factors. *Hypertens Res* 2011; **34**: 281–285.
4 Sica DA, Carter B, Cushman W, Hamm L. Thiazide and loop diuretics. *J Clin Hypertens* 2011; **13**: 639–643.
5 Kawano Y, Yoshida K, Kawamura M, Yoshimi H, Ashida T, Abe H, Imanishi M, Kimura G, Kojima S, Kuramochi M. Sodium and noradrenaline in cerebrospinal fluid and blood in salt-sensitive and non-salt-sensitive essential hypertension. *Clin Exp Pharmacol Physiol* 1992; **19**: 235–241.
6 Adrogue HJ, Madias NE. Sodium and potassium in the pathogenesis of hypertension. *N Engl J Med* 2007; **356**: 1966–1978.
7 Huang BS, Amin MS, Leenen FH. The central role of the brain in salt-sensitive hypertension. *Curr Opin Cardiol* 2006; **21**: 295–304.
8 Huang BS, Van Vliet BN, Leenen FH. Increases in CSF [Na^+] precede the increases in blood pressure in dahl S rats and SHR on a high-salt diet. *Am J Physiol Heart Circ Physiol* 2004; **287**: H1160–H1166.
9 Takahashi H, Yoshika M, Komiyama Y, Nishimura M. The central mechanism underlying hypertension: a review of the roles of sodium ions, epithelial sodium channels, the renin-angiotensin-aldosterone system, oxidative stress and endogenous digitalis in the brain. *Hypertens Res* 2011; **34**: 1147–1160.

10 Fujita M, Ando K, Nagae A, Fujita T. Sympathoexcitation by oxidative stress in the brain mediates arterial pressure elevation in salt-sensitive hypertension. *Hypertension* 2007; **50**: 360–367.
11 Huang BS, White RA, Jeng AY, Leenen FH. Role of central nervous system aldosterone synthase and mineralocorticoid receptors in salt-induced hypertension in dahl salt-sensitive rats. *Am J Physiol Regul Integr Comp Physiol* 2009; **296**: R994–R1000.
12 Huang BS, Wang H, Leenen FH. Enhanced sympathoexcitatory and pressor responses to central Na^+ in dahl salt-sensitive vs. -resistant rats. *Am J Physiol Heart Circ Physiol* 2001; **281**: H1881–H1889.
13 Huang BS, White RA, Ahmad M, Jeng AY, Leenen FH. Central infusion of aldosterone synthase inhibitor prevents sympathetic hyperactivity and hypertension by central Na^+ in wistar rats. *Am J Physiol Regul Integr Comp Physiol* 2008; **295**: R166–R172.
14 Praetorius J. Water and solute secretion by the choroid plexus. *Pflugers Arch* 2007; **454**: 1–18.
15 Brown PD, Davies SL, Speake T, Millar ID. Molecular mechanisms of cerebrospinal fluid production. *Neuroscience* 2004; **129**: 957–970.
16 Amin MS, Wang HW, Reza E, Whitman SC, Tuana BS, Leenen FH. Distribution of epithelial sodium channels and mineralocorticoid receptors in cardiovascular regulatory centers in rat brain. *Am J Physiol Regul Integr Comp Physiol* 2005; **289**: R1787–R1797.
17 Canessa CM, Schild L, Buell G, Thorens B, Gautschi I, Horisberger JD, Rossier BC. Amiloride-sensitive epithelial Na^+ channel is made of three homologous subunits. *Nature* 1994; **367**: 463–467.
18 Schild L. The epithelial sodium channel and the control of sodium balance. *Biochim Biophys Acta* 2010; **1802**: 1159–1165.
19 Wulff P, Vallon V, Huang DY, Volkl H, Yu F, Richter K, Jansen M, Schlunz M, Klingel K, Loffing J, Kauselmann G, Bosl MR, Lang F, Kuhl D. Impaired renal Na^+ retention in the sgk1-knockout mouse. *J Clin Invest* 2002; **110**: 1263–1268.
20 Pearce D, Kleyman TR. Salt, sodium channels, and SGK1. *J Clin Invest* 2007; **117**: 592–595.
21 Zhang W, Xia X, Reisenauer MR, Rieg T, Lang F, Kuhl D, Vallon V, Kone BC. Aldosterone-induced Sgk1 relieves Dot1a-Af9-mediated transcriptional repression of epithelial na+ channel alpha. *J Clin Invest* 2007; **117**: 773–783.
22 Quinkler M, Zehnder D, Eardley KS, Lepenies J, Howie AJ, Hughes SV, Cockwell P, Hewison M, Stewart PM. Increased expression of mineralocorticoid effector mechanisms in kidney biopsies of patients with heavy proteinuria. *Circulation* 2005; **112**: 1435–1443.
23 Camargo MJ, von Lutterotti N, Campbell Jr WG, Pecker MS, James GD, Timmermans PB, Laragh JH. Control of blood pressure and end-organ damage in maturing salt-loaded stroke-prone spontaneously hypertensive rats by oral angiotensin II receptor blockade. *J Hypertens* 1993; **11**: 31–40.
24 Endemann DH, Touyz RM, Iglarz M, Savoia C, Schiffrin EL. Eplerenone prevents salt-induced vascular remodeling and cardiac fibrosis in stroke-prone spontaneously hypertensive rats. *Hypertension* 2004; **43**: 1252–1257.
25 Nishihara M, Hirooka Y, Matsukawa R, Kishi T, Sunagawa K. Oxidative stress in the rostral ventrolateral medulla modulates excitatory and inhibitory inputs in spontaneously hypertensive rats. *J Hypertens* 2012; **30**: 97–106.
26 Matsukawa R, Hirooka Y, Nishihara M, Ito K, Sunagawa K. Neuregulin-1/ErbB signaling in rostral ventrolateral medulla is involved in blood pressure regulation as an antihypertensive system. *J Hypertens* 2011; **29**: 1735–1742.
27 Ito K, Kimura Y, Hirooka Y, Sagara Y, Sunagawa K. Activation of rho-kinase in the brainstem enhances sympathetic drive in mice with heart failure. *Auton Neurosci* 2008; **142**: 77–81.
28 Schad H, Seller H. Influence of intracranial osmotic stimuli on renal nerve activity in anaesthetized cats. *Pflugers Arch* 1975; **353**: 107–121.
29 Kumagai H, Oshima N, Matsuura T, Iigaya K, Imai M, Onimaru H, Sakata K, Osaka M, Onami T, Takimoto C, Kamayachi T, Itoh H, Saruta T. Importance of rostral ventrolateral medulla neurons in determining efferent sympathetic nerve activity and blood pressure. *Hypertens Res* 2012; **35**: 132–141.
30 Denton DA, McKinley MJ, Weisinger RS. Hypothalamic integration of body fluid regulation. *Proc Natl Acad Sci USA* 1996; **93**: 7397–7404.
31 Cato MJ, Toney GM. Angiotensin II excites paraventricular nucleus neurons that innervate the rostral ventrolateral medulla: An *in vitro* patch-clamp study in brain slices. *J Neurophysiol* 2005; **93**: 403–413.
32 Li DP, Chen SR, Pan HL. Angiotensin II stimulates spinally projecting paraventricular neurons through presynaptic disinhibition. *J Neurosci* 2003; **23**: 5041–5049.
33 Hirooka Y. Oxidative stress in the cardiovascular center has a pivotal role in the sympathetic activation in hypertension. *Hypertens Res* 2011; **34**: 407–412.
34 Wang HW, Amin MS, El-Shahat E, Huang BS, Tuana BS, Leenen FH. Effects of central sodium on epithelial sodium channels in rat brain. *Am J Physiol Regul Integr Comp Physiol* 2010; **299**: R222–R233.
35 Gabor A, Leenen FH. Mechanisms in the PVN mediating local and central sodium-induced hypertension in wistar rats. *Am J Physiol Regul Integr Comp Physiol* 2009; **296**: R618–R630.
36 Shi P, Martinez MA, Calderon AS, Chen Q, Cunningham JT, Toney GM. Intra-carotid hyperosmotic stimulation increases fos staining in forebrain organum vasculosum laminae terminalis neurones that project to the hypothalamic paraventricular nucleus. *J Physiol* 2008; **586**: 5231–5245.
37 Suzuki J, Ogawa M, Tamura N, Maejima Y, Takayama K, Maemura K, Honda K, Hirata Y, Nagai R, Isobe M. A critical role of sympathetic nerve regulation for the treatment of impaired daily rhythm in hypertensive Dahl rats. *Hypertens Res* 2010; **33**: 1060–1065.
38 Brooks VL, Haywood JR, Johnson AK. Translation of salt retention to central activation of the sympathetic nervous system in hypertension. *Clin Exp Pharmacol Physiol* 2005; **32**: 426–432.
39 Koga Y, Hirooka Y, Araki S, Nozoe M, Kishi T, Sunagawa K. High salt intake enhances blood pressure increase during development of hypertension via oxidative stress in rostral ventrolateral medulla of spontaneously hypertensive rats. *Hypertens Res* 2008; **31**: 2075–2083.
40 Ito K, Hirooka Y, Sunagawa K. Blockade of mineralocorticoid receptors improves salt-induced left-ventricular systolic dysfunction through attenuation of enhanced sympathetic drive in mice with pressure overload. *J Hypertens* 2010; **28**: 1449–1458.
41 Gomez-Sanchez EP, Ahmad N, Romero DG, Gomez-Sanchez CE. Is aldosterone synthesized within the rat brain? *Am J Physiol Endocrinol Metab* 2005; **288**: E342–E346.
42 Geerling JC, Loewy AD. Aldosterone in the brain. *Am J Physiol Renal Physiol* 2009; **297**: F559–F576.
43 Funder JW. Mineralocorticoid receptors: distribution and activation. *Heart Fail Rev* 2005; **10**: 15–22.
44 Shibata S, Nagase M, Yoshida S, Kawarazaki W, Kurihara H, Tanaka H, Miyoshi J, Takai Y, Fujita T. Modification of mineralocorticoid receptor function by Rac1 GTPase: implication in proteinuric kidney disease. *Nat Med* 2008; **14**: 1370–1376.
45 Duc C, Farman N, Canessa CM, Bonvalet JP, Rossier BC. Cell-specific expression of epithelial sodium channel alpha, beta, and gamma subunits in aldosterone-responsive epithelia from the rat: localization by in situ hybridization and immunocytochemistry. *J Cell Biol* 1994; **127**: 1907–1921.
46 Nakagaki T, Hirooka Y, Matsukawa R, Nishihara M, Nakano M, Ito K, Hoka S, Sunagawa K. Activation of mineralocorticoid receptors in the rostral ventrolateral medulla is involved in hypertensive mechanisms in stroke-prone spontaneously hypertensive rats. *Hypertens Res* 2012; **35**: 470–476.
47 Kumar NN, Goodchild AK, Li Q, Pilowsky PM. An aldosterone-related system in the ventrolateral medulla oblongata of spontaneously hypertensive and wistar-kyoto rats. *Clin Exp Pharmacol Physiol* 2006; **33**: 71–75.
48 Amin MS, Reza E, Wang H, Leenen FH. Sodium transport in the choroid plexus and salt-sensitive hypertension. *Hypertension* 2009; **54**: 860–867.
49 Kolla V, Litwack G. Transcriptional regulation of the human Na/K ATPase via the human mineralocorticoid receptor. *Mol Cell Biochem* 2000; **204**: 35–40.

Original Article

Pitavastatin-Incorporated Nanoparticle-Eluting Stents Attenuate In-Stent Stenosis without Delayed Endothelial Healing Effects in a Porcine Coronary Artery Model

Noriaki Tsukie[1], Kaku Nakano[1], Tetsuya Matoba[1], Seigo Masuda[1], Eiko Iwata[1], Miho Miyagawa[1], Gang Zhao[3], Wei Meng[3], Junji Kishimoto[2], Kenji Sunagawa[1] and Kensuke Egashira[1]

[1]Department of Cardiovascular Medicine, Graduate School of Medical Sciences, Kyushu University, Fukuoka, Japan
[2]Digital Medicine Initiative, Graduate School of Medical Sciences, Kyushu University, Fukuoka, Japan
[3]Department of Cardiovascular Medicine, 6th People's Hospital, Shanghai Jiatong University, Shanghai, China

Aim: The use of currently marketed drug-eluting stents presents safety concerns including increased late thrombosis, which is thought to result mainly from delayed endothelial healing effects (impaired re-endothelialization resulting in abnormal inflammation and fibrin deposition). We recently developed a bioabsorbable polymeric nanoparticle (NP)-eluting stent using a novel cationic electrodeposition technology. Statins are known to inhibit the proliferation of vascular smooth muscle cells (VSMC) and to promote vascular healing. We therefore hypothesized that statin-incorporated NP-eluting stents would attenuate in-stent stenosis without delayed endothelial healing effects.
Methods: Among six marketed statins, pitavastatin (Pitava) was found to have the most potent effects on VSMC proliferation and endothelial regeneration *in vitro*. We thus formulated a Pitava-NP-eluting stent (20 μg Pitava per stent).
Results: In a pig coronary artery model, Pitava-NP-eluting stents attenuated in-stent stenosis as effectively as polymer-coated sirolimus-eluting stents (SES). At SES sites, delayed endothelial healing effects were noted, whereas no such effects were observed in Pitava-NP-eluting stent sites.
Conclusion: Pitava-NP-eluting stents attenuated in-stent stenosis as effectively as SES without the delayed endothelial healing effects of SES in a porcine coronary artery model. This nanotechnology platform could be developed into a safer and more effective device in the future.

J Atheroscler Thromb, 2013; 20:32-45.

Key words; Statin, Nanotechnology, Drug delivery system, Signal transduction

Introduction

Increased risk of late in-stent thrombosis resulting in acute coronary syndrome (unstable angina, acute myocardial infarction and death) after the use of drug-eluting stent (DES) devices has become a major safety concern[1-3]. These adverse effects are thought to result mainly from the anti-healing effects of the drugs (sirolimus and paclitaxel) on endothelial cells, leading to impaired re-endothelialization, excessive inflammation, proliferation and fibrin deposition[4-6]. These "anti-healing" drugs are used in most newer generation DESs, leading to continued safety concerns; therefore, the cellular and/or molecular targeting of both VSMC proliferation and re-endothelialization is an essential requirement for the development of more efficient and safer DESs. The use of an anti-healing approach that accelerates re-endothelialization, protects against thrombosis and decreases restenosis is warranted. Comparator analysis of endothelial cell coverage in four marketed polymeric DESs in rabbits has demonstrated a disparity in arterial healing; notably, all DESs examined showed a lack of endothelial anticoagulant function, independent of endothelial coverage[7].

Address for correspondence: Kensuke Egashira, Department of Cardiovascular Medicine, Graduate School of Medical Science, Kyushu University, 3-1-1, Maidashi, Higashi-ku, Fukuoka 812-8582, Japan
E-mail: egashira@cardiol.med.kyushu-u.ac.jp
Received: March 18, 2012
Accepted for publication: June 21, 2012

We hypothesized that HMG-CoA reductase inhibitors, so-called statins, are appropriate candidate drugs for the anti-healing strategy because the vascular endothelium is a major target for the pleiotropic (non-LDL-related) vasculoprotective effects of statins[8]. In cell culture experiments *in vitro*, statins reportedly promoted endothelial regeneration and inhibited VSMC proliferation and tissue factor expression[8, 9]. Systemic administration of statins has been reported to inhibit balloon injury-induced and in-stent neointima formation in non-hypercholesterolemic animals. Most of these beneficial effects of statins on neointima formation in animals, however, were observed following daily administration of high doses[8, 10] (rosuvastatin 20 mg/kg per day[11], pitavastatin 40 mg/kg per day[12], simvastatin 40 mg/kg per day[13]); this may lead to serious adverse side effects in a clinical setting. Furthermore, it has been reported that the use of polymer-coated stents with atorvastatin or cerivastatin has no consistent effect on neointima formation in a porcine in-stent stenosis model[14, 15]. Randomized clinical studies in humans have reported no definite effects of statins within the clinical dose range with respect to indices of restenosis after coronary balloon angioplasty[16-19] or coronary stenting[20, 21]; therefore, preventing in-stent restenosis via statin-mediated "anti-healing" effects requires an efficient local drug delivery system.

To overcome this problem, we recently introduced nanoparticles (NP) formulated from the bioabsorbable polymer poly(DL-lactide-co-glycolide) (PLGA) and succeeded in formulating an NP-eluting stent by a cationic electrodeposition coating technology[22]. Therefore, we hypothesized that statin-NP-eluting stents could be an innovative therapeutic "anti-healing" strategy for treating in-stent stenosis *in vivo*.

Materials and Methods

Statins (simvastatin, pitavastatin, atorvastatin, rosuvastatin, fluvastatin, and pravastatin) were purchased, extracted from products, and purified.

Human Coronary Artery Smooth Muscle Cell Proliferation

Human coronary artery smooth muscle cells (SMC) were cultured as previously described[22, 23] and plated into 96-well culture plates at 1×10^4 cells per well in SMGM2. Proliferation was stimulated by adding human PDGF at 10 ng/mL (Sigma, Tokyo, Japan) or 10% FBS to each well. Either vehicle alone or several concentrations of statins, sirolimus, or paclitaxel were added to the well. Cellular proliferation responses were determined by evaluating the 5'-bromo-2'-deoxyuridine (BrdU) incorporation rate and/or by a cell counting method, as previously described[22, 23].

Human Endothelial Cell Scratch Motility Assay

A scratch motility assay using human umbilical vein endothelial cells (HUVEC) was performed to assess the re-endothelialization response following endothelial denudation. HUVECs were seeded in collagen I-coated 24-well plates at a density of 2×10^4 cells per well and grown to confluence with EGM2. The monolayers were wounded with a pipet tip, washed with PBS twice, photographed and incubated at 37℃ with EBM containing 0.5% BSA containing $VEGF_{165}$ (10 ng/mL, R & D) in the presence or absence of statins, sirolimus, or paclitaxel. After five hours, cells were photographed, and the number of cells that had migrated into the wounded area was counted.

Western Blot Analysis

Human aortic endothelial cells (HAEC) were cultured to confluence in 3 cm dishes and rendered quiescent for 24 hours before stimulation with 1 U/mL thrombin (Sigma). Sirolimus, paclitaxel (both Sigma), and pitavastatin were added to the cells one hour before thrombin (1 U/mL) stimulation. Tissue factor protein expression was determined by Western blot analysis. In another set of experiments, sirolimus was added to HAEC and effects of pitavastatin on sirolimus-induced changes in endothelial nitric oxide synthase (eNOS) and protein kinase B (Akt) protein were examined.

Cell extracts (20 μg) were resolved on 10% reducing SDS-PAGE gels and blotted onto nitrocellulose membranes (Bio-Rad, Hercules, CA). Antibodies against human tissue factor (Calbiochem), phosphorylated-Akt (ser473), phosphorylated-eNOS (ser1177), Akt (Cell Signaling), eNOS (Affinity BioReagents) were used. Immune complexes were visualized with horseradish peroxidase-conjugated secondary antibodies (Pierce, Rockford, IL) using the ECL Plus system (Amersham Biosciences) and were detected with the ECL Detection Kit (Amersham). Blots were normalized against GAPDH expression (Sigma).

Preparation of Cationic PLGA Nanoparticles (NP) with Surface Modification with Chitosan

A lactide/glycolide copolymer (PLGA) with an average molecular weight of 20,000 and a lactide to glycolide copolymer ratio of 75:25 (PLGA7520; Wako Pure Chemical Industries, Osaka, Japan) was used as wall material for the NPs because the bioabsorption

half-life of this product is two weeks in rat tissue (manufacturer's instructions). PLGA NPs incorporated with the fluorescent marker fluorescein isothiocyanate (FITC; Dojindo laboratories, Kumamoto, Japan) or with pitavastatin were prepared by a previously reported emulsion solvent diffusion method in purified water[22]. FITC- and pitavastatin-loaded PLGA NPs contained 5.0% (w/v) FITC and 6.5% (w/v) pitavastatin, respectively, and were preserved as freeze-dried material. The mean particle size was analyzed by the light scattering method (Microtrack UPA150; Nikkiso, Tokyo, Japan). The average diameter of the PLGA NPs was 226 ± 29 nm. The surface charge (zeta potential) was also analyzed by Zetasizer Nano (Sysmex, Hyogo, Japan) and was found to be cationic (+36 mV at pH 4.4).

Preparation of NP-Eluting Stents by Cationic Electrodeposition Coating Technology

The 15 mm-long stainless-steel, balloon-expandable stents (Multilink) were ultrasonically cleaned in acetone, ethanol, and demineralized water. The cationic electrodeposited coating was prepared on cathodic stents in NP solution at a concentration of 5 g/L in distilled water with a current maintained between 2.0 and 10.0 mA by a direct current power supply (DC power supply; Nippon Stabilizer Co, Tokyo, Japan) for different periods under sterile conditions.28, 31 The coated stents were then rinsed with demineralized water and dried under a vacuum overnight. This electrodeposition coating procedure produced a coating of approximately 367 ± 77 μg of the PLGA NPs per stent and 20 ± 4 μg of pitavastatin per stent (n = 12). The surfaces of some NP-coating stents were examined with scanning electron microscopy (JXM8600; JEOL, Tokyo, Japan), and it was confirmed that the NPs were structurally intact and cohesive[22].

Analysis of Endothelial Surface Coverage by en Face Scanning Electron Microscopy

For evaluation of endothelial coverage, stents were excised seven days after implantation. The stented arteries were fixed *in situ* with 10% neutral-buffered formalin after perfusion with lactated Ringer's solution to remove blood. The samples were further fixed by immersion and then bisected longitudinally with one half processed for scanning electron microscopy (SEM).

Composites of serial en face SEM images acquired at low power (×15 magnification) were digitally assembled to provide a complete view of the entire luminal stent surface. The images were further enlarged (×200 magnification), allowing direct visualization of endothelial cells. The extent of endothelial surface coverage above and between stent struts was traced and measured by morphometry software. The results are expressed as a percentage of the total surface area above or between struts or the total and percentage area lacking coverage at each repeated crown along the longitudinal axis from the proximal to the distal orientation. Endothelial cells were identified as sheets of spindle- or polygonal-shaped monolayers in close apposition, a distinguishing feature from other cell types in en face preparations[24]. By contrast, intimal smooth muscle cells showed elongated processes and were generally stacked in disorganized or haphazard layers[24]. Other adherent cells present on stent surfaces included platelets, characteristically 1 to 2 μm in size with an irregular discoid appearance, and inflammatory cells, which were round and varied from 7 to 10 μm in diameter with a ruffled surface. Struts uncovered by endothelium were completely bare or contained thrombi consisting of focal platelet and fibrin aggregates intermixed with red blood cells and inflammatory cells.

Measurements of Pitavastatin Concentration in Serum and Arterial Tissue

Concentrations of pitavastatin in serum and stented arterial tissue were measured at predetermined time points using a column-switching high performance liquid chromatography (HPLC) system as previously reported[25]. Briefly, the column-switching HPLC system consists of two LC-10AD pumps, a SIL-10A auto-sampler, a CTO-10A column oven, a six-port column-switching valve, and an SPD-10A UV-detector (all from Shimadzu, Kyoto, Japan). The column temperature was maintained at 40℃. Pre-prepared serum or tissue homogenate sample solutions were injected from the auto-sampler into the HPLC system, and statin in the sample solutions was detected at 250 nm with a UV detector. The detected peak area was measured with Lc solution software (Shimadzu, Kyoto, Japan).

Animal Preparation and Stent Implantation

All *in vivo* experiments were reviewed and approved by the Committee on Ethics in Animal Experiments, Kyushu University Faculty of Medicine, according to the Guidelines of the American Physiological Society.

Domestic male pigs (Kyudo, Tosu, Japan; aged 2 to 3 months and weighing 25 to 30 kg) received orally aspirin (330 mg/day) and ticlopidine (200 mg/day) until euthanasia from 3 days before stent implantation

Table 1. Inhibitory effects of 6 commercially available statins on proliferation of human coronary artery smooth muscle cells

	IC_{50} values (nmol/L)	efficacy ratio	95% Wald confidence intervals	*p* value
pitavastatin	193	1	–	–
fluvastatin	836	0.230	0.119, 0.446	<0.001
atorvastatin	2512	0.077	0.039, 0.150	<0.001
simvastatin	3951	0.049	0.023, 0.104	<0.001
rosuvastatin	Not calculated	Not calculated	Not calculated	Not calculated
pravastatin	Not calculated	Not calculated	Not calculated	Not calculated

$n=6$ each. *p* values versus pitavastatin by Wald tests in 4-parameter logistic regression model.

procedure. Animals were anesthetized with ketamine hydrochloride (15 mg/kg, IM) and pentobarbital (20 mg/kg, IV). They were then intubated and mechanically ventilated with room air. A preshaped Judkins catheter was inserted into the carotid artery and advanced into the orifice of the left coronary artery. After systemic heparinization (100 IU/kg) and intracoronary administration of nitroglycerin, coronary angiography of the left coronary artery was performed with the use of contrast media (iopamidol 370) in a left oblique view with the angiography system (Toshiba Medical, Tokyo, Japan).

Animals were divided into groups, which underwent deployment of either non-coated bare metal stents (1 week: $n=3$, 4 weeks: $n=12$), FITC-incorporated NP-eluting stents (4 weeks: $n=12$), pitavastatin-incorporated NP-eluting stents (1 week: $n=3$, 4 weeks: $n=12$), or sirolimus-eluting stents (Cypher; 3 mm × 15 mm) (1 week: $n=3$, 4 weeks: $n=12$) in the left anterior descending (LAD) or the left circumflex (LCx) coronary arteries. After arterial blood samples were taken, animals were given a lethal dose of anesthesia after 1 or 4 weeks, and the stented arterial sites and contralateral non-stented sites were excised for biochemical, immunohistochemical, and morphometric analyses.

As another set of experiments, animals were treated with intracoronary administration of pitava-NP at 300 μg (a similar dose to that coated on pitavastatin-NP eluting stent, 4 weeks: $n=6$) and 3000 μg (10x dose coated on pitavastatin-NP eluting stent, 4 weeks: $n=6$) containing 20 and 200 μg pitavastatin, respectively, immediately after deployment of bare metal stents. Pitava-NPs were diluted with 10 mL saline. Intracoronary administration of 10 mL saline was used as a control experiment (4 weeks: $n=5$).

A segment with a mean coronary diameter of 2.5 mm was selected by using quantitative coronary angiography with a stent-to-artery ratio of approximately 1.1 : 1.2. A balloon catheter mounted with a stent was then advanced to the pre-selected coronary segments for deployment over a standard guide-wire. The balloon catheter was inflated at 15 atm for 60 seconds once and was then slowly withdrawn, leaving the stent in place.

Quantitative coronary angiography (Toshiba Medical, Tokyo, Japan) was performed before, immediately after, and 4 weeks after stent implantation to examine the coronary arterial diameter at stented and non-stented sites. The image of a Judkins catheter was used as reference diameter. Arterial pressure, heart rate, and ECG were continuously monitored and recorded on a recorder.

Histopathological Study

Four weeks after the coronary angiographic study, animals were euthanized with a lethal dose of sodium pentobarbital (40 mg/kg intravenously), and histological analysis was performed. The left coronary artery was perfused with 10% buffered formalin at 120 mmHg and fixed for 24 hours. The stented artery segments were isolated and processed as described previously[26]. The segment was divided into two parts at the center of the stent and then embedded in methyl methacrylate mixed with n-butyl methacrylate to allow for sectioning through the metal stent struts. Serial sections were stained with elastica van Gieson and hematoxylin-eosin (HE). The neointimal area, the area within the internal elastic lamina (IEL), and the lumen area were measured by computerized morphometry, which was carried out by a single observer who was blinded to the experimental protocol. All images were captured by an Olympus microscope equipped with a digital camera (HC-2500) and were analyzed using Adobe Photoshop 6.0 and Scion Image 1.62 software. The injury, inflammation, fibrin, hemorrhage and re-endothelialization scores were determined at each strut site, and mean values were calculated for each stented segment.

Statistical Analysis

Data are expressed as the means ± SE. Statistical analysis of differences between two groups was performed with the unpaired *t*-test, and differences among groups were analyzed using ANOVA and multiple comparison tests.

Efficacy ratios (IC_{50} values) of the statins were tested using Wald tests in a four-parameter logistic regression model. Point estimates and Wald 95% confidence intervals for efficacy ratios were calculated. Statistical calculations were performed with SAS preclinical package software version 9.1.3 (SAS Institute Inc., Japan, Tokyo). *P* values <0.05 were considered significant.

Results

Effects of Statins on Human Coronary Artery Smooth Muscle Cell Proliferation and Endothelial Cell Scratch Motility Assay

To incorporate statins into the NP-eluting stent design, the effects of statins were compared. In the human CASMC proliferation assay (% inhibition of BrdU index), hydrophilic statins (rosuvastatin and pravastatin) had no effects on PDGF-induced proliferation; thus, calculation of the IC_{50} value was impossible for those statins (**Table 1**). By contrast, the other four statins showed concentration-dependent inhibition. The IC_{50} values of the four statins are shown in **Table 1**, which indicates that the value for pitavastatin is lowest.

In the human endothelial cell scratch motility assay (re-endothelialization *in vitro*), only pitavastatin increased the re-endothelialization response following scratch injury; the other five statins showed no such effects (**Fig. 1**). In addition, there was no difference in the re-endothelialization response among the five statins.

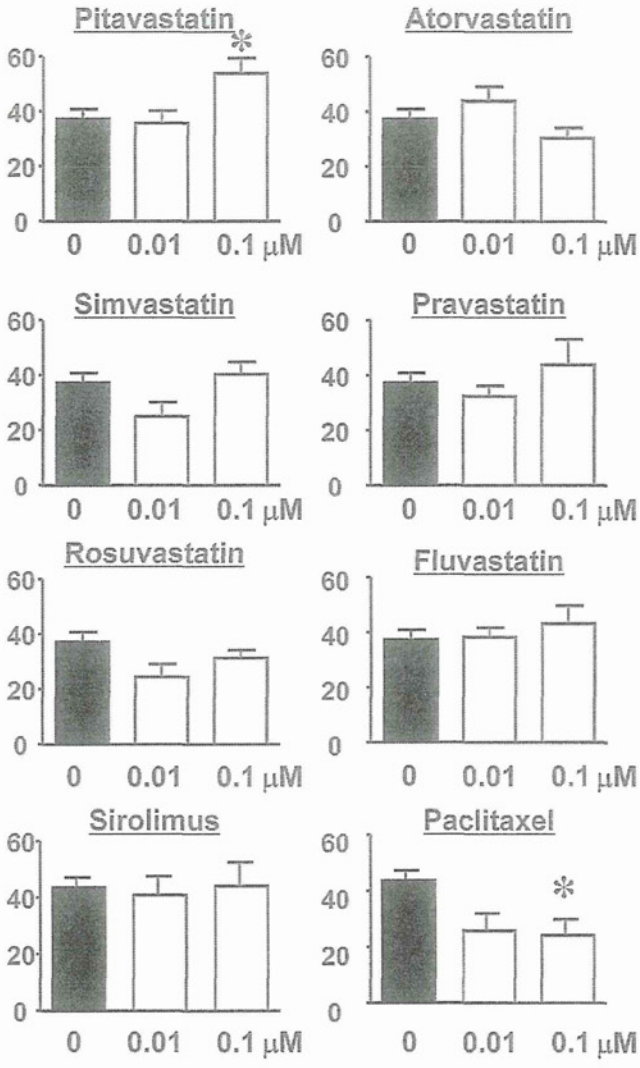

Fig. 1. Human umbilical vein endothelial cell scratch motility assay *in vitro*. Vertical axis denotes the number of migrated cells into the scratched area. $^*p<0.05$ vs no treatment by one-way ANOVA followed with Dunnett's multiple comparison test ($n=6$-8 each).

Effects of Pitavastatin, Sirolimus, and Paclitaxel on Human Coronary Artery Smooth Muscle Cell Proliferation, Endothelial Cell Scratch Motility Assay, and Tissue Factor Expression in Human Endothelial Cells

To incorporate pitavastatin into the NP-eluting stent design, the effects of pitavastatin were then compared with those of sirolimus and paclitaxel. All three drugs inhibited human CASMC proliferation (**Fig. 2**). In the human endothelial cell scratch motility assay, sirolimus did not affect the re-endothelialization response, whereas the response was significantly delayed in paclitaxel-treated endothelial cells (**Fig. 1**).

Because tissue factor has a primary role in stent thrombosis, its protein expression was examined in human endothelial cells. As previously reported by others[27], both sirolimus and paclitaxel enhanced the thrombin-induced tissue factor expression (**Fig. 2**). By contrast, pitavastatin inhibited tissue factor expression (**Fig. 2**).

Effects of Pitavastatin on Sirolimus-Induced Down Regulation of eNOS in Human Endothelial Cells

Sirolimus down regulated phosphorylated-eNOS and decreased phosphorylated Akt (a representative down stream signal of eNOS), while sirolimus had no effects on eNOS and Akt protein expression (**Fig. 3**).

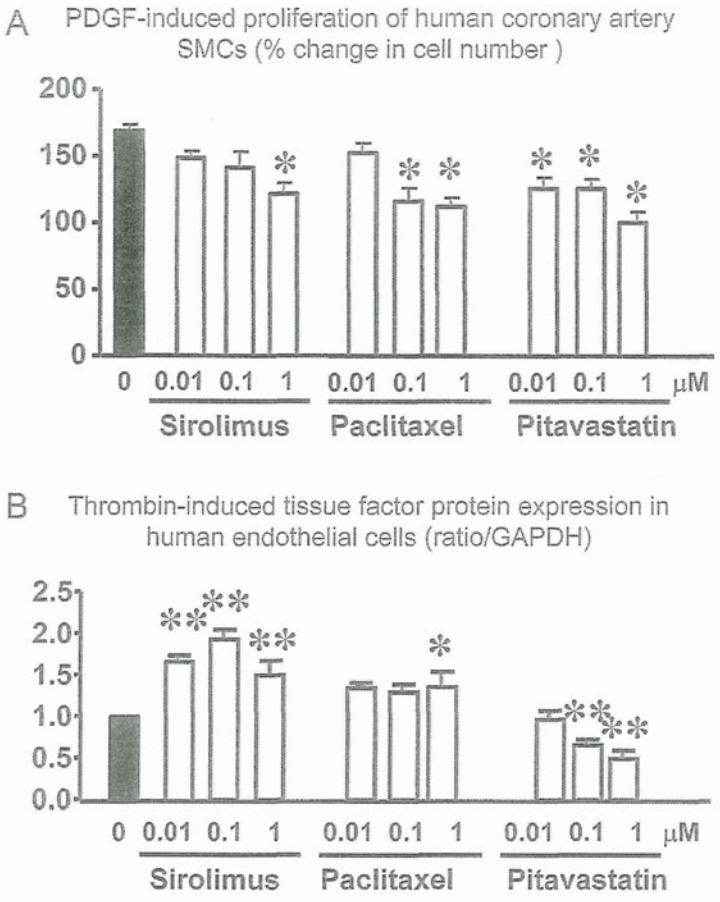

Fig. 2. Effects of pitavastatin, sirolimus, and paclitaxel on human CASMC proliferation and human AEC tissue factor expression.

A, PDGF-induced proliferation (% increase in cell number) of human CASMCs. Data are the mean ± SEM ($n=6$ each). $^*p<0.01$ versus control by one-way ANOVA followed with Dunnett's multiple comparison test. B, Thrombin-induced tissue factor protein expression in human AECs. Data are the mean ± SEM ($n=6$ each). $^*p<0.01$ versus thrombin alone by one-way ANOVA followed with Dunnett's multiple comparison test.

Pitavastatin nearly normalized the sirolimus-induced decrease in p-eNOS and p-Akt protein expression.

Effects of Pitavastatin and Pitavastatin-NP on Human CASMC Proliferation

Both pitavastatin and pitavastatin-NP inhibited the FBS-induced proliferation of human CASMC. The inhibitory activities of pitavastatin-NP were greater than those of 0.01, 0.1, and 1 μM pitavastatin only (**Fig. 4**).

Effects of Pitavastatin-NP-Eluting Stents and Sirolimus-Eluting Stents on Neointima Formation Four Weeks after Stent Implantation

Two animals in the control bare metal stent group died suddenly between weeks three and four; therefore, these animals were excluded from angiographic and histopathological analyses, which were performed in 34 pigs (10 in the control bare metal stent group, 12 in the FITC-NP-eluting stent group, 12 in the pitavastatin-NP eluting stent group, and 12 in the sirolimus-eluting stent group).

Quantitative coronary arteriography revealed that (1) there was no significant difference in the coronary diameter before and immediately after stent implantation or in the stent-to-artery ratio among the four groups and (2) the coronary diameter was less in the control bare metal and the FITC-NP-eluting stent sites than in the pitavastatin-NP-eluting stent and sirolimus-eluting stent sites four weeks after stenting

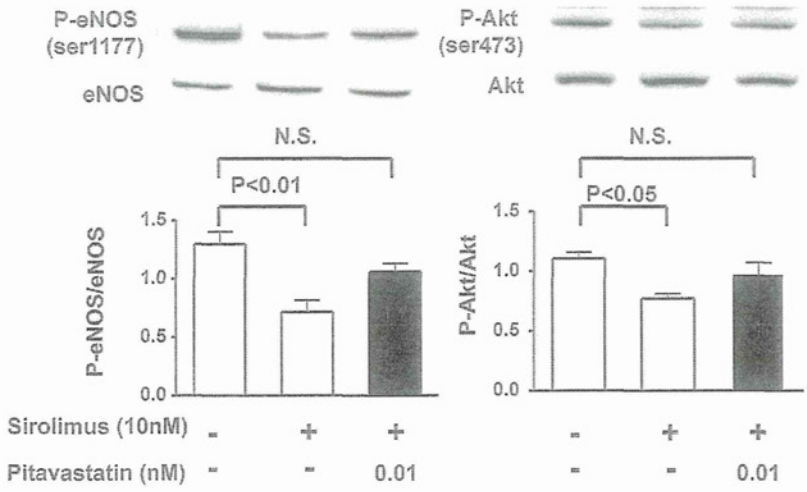

Fig. 3. Effects of pitavastatin on sirolimus-induced down regulation of eNOS and Akt (a representative down stream signal of eNOS) in human aortic endothelial cells. Pitavastatin normalized sirolimus-induced decrease in phosphorylated (activated) eNOS and Akt. Data are the mean ± SEM ($n=6$ each). $p<0.05$ or 0.01 versus no treatment by one-way ANOVA followed with Dunnett's multiple comparison test.

(**Table 2**). Thus, the angiographically examined in-stent stenosis was less in the pitavastatin-NP group than in the control and FITC-NP groups. The sirolimus-eluting stent showed similar inhibitory effects on markers of in-stent stenosis.

Histological analysis demonstrated that a significant in-stent neointima formed similarly at the bare metal stent and FITC-NP-eluting stent sites (**Fig. 5**). Quantitative analysis demonstrated that pitavastatin-NP-eluting stents attenuated in-stent neointima formation as effectively as sirolimus-eluting stents.

Effects of Pitavastatin-NP-Eluting Stents Versus Sirolimus-Eluting Stents on Inflammation and Fibrin Deposition

Micrographs of coronary artery cross-sections stained with hematoxylin-eosin from FITC-NP-eluting, pitavastatin-NP-eluting, and sirolimus-eluting stent groups are shown in **Fig. 6**. A semi-quantitative histological scoring system demonstrated that there was no significant difference in the injury score among the four groups four weeks after stenting (**Table 3**).

Inflammatory cells consisting mainly of macrophages were recruited around the stent wire and into the neointimal layer in all four sites; however, the inflammation score was significantly less at the pitavastatin-NP-eluting stent site than in the bare metal stent site (**Table 3**). At the sirolimus-eluting stent site, the inflammation score was greater than at the bare metal stent and pitavastatin-NP-eluting stent sites (**Table 3**).

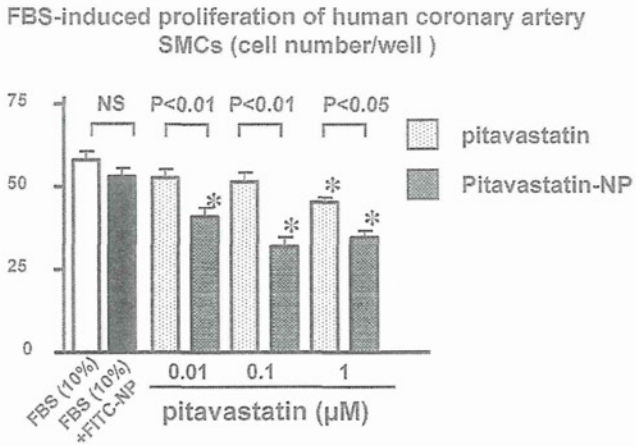

Fig. 4. Effects of pitavastatin and pitavastatin-NP on the FBS-induced proliferation of human CASMCs. Data are the mean ± SEM ($n=6$ each). $^*p<0.01$ versus no treatment by one-way ANOVA followed with Dunnett's multiple comparison test.

Minor fibrin deposition was observed at bare metal, FITC-NP-eluting, and pitavastatin-NP-eluting stent sites (**Table 3**). At the sirolimus-eluting stent site, the fibrin score was significantly higher than at the bare metal stent site, and this difference was even more significant when compared with the pitavastatin-NP-eluting stent site.

To determine whether the therapeutic effects of

Table 2. Coronary angiographic parameters (coronary artery diameter, in-stent stenosis) before, immediately after, and 4 weeks after stent implantation in porcine coronary artery

	BMS ($n=10$)	FITC-NP stent ($n=12$)	Pitavastatin -NP stent ($n=12$)	SES ($n=12$)	p value
Coronary diameter before stent implantation	2.19 ± 0.04	2.25 ± 0.05	2.41 ± 0.06	2.42 ± 0.10	NS
Coronary diameter immediately after stent implantation	2.70 ± 0.06	2.75 ± 0.05	2.79 ± 0.03	2.89 ± 0.04	NS
Stent-to-artery ratio immediately after stent implantation	1.20 ± 0.02	1.22 ± 0.03	1.13 ± 0.02	1.19 ± 0.04	NS
Coronary diameter 4 weeks after stent implantation	1.45 ± 0.13	1.51 ± 0.10	2.02 ± 0.12*	2.02 ± 0.15*	0.0025
Angiographically-examined in-stent restenosis 4 weeks after stent implantation (% diameter stenosis)	42.9 ± 4.9	46.0 ± 3.4	25.8 ± 3.5*	27.2 ± 3.7*	0.0003

Data are the mean ± SEM. NS = not significant
*$p<0.05$ versus control bare metal stent by Bonferroni's multiple comparison tests

the pitavastatin-NP-eluting stent are mediated by local or systemic mechanisms, effects of intracoronary administration of pitavastatin-NP on histopathological features after deployment of bare metal stents were examined (**Table 4**). Pitavastatin-NP at 300 μg showed no therapeutic effects on indices of in-stent stenosis and adverse effects on histopathological scoring. Pitavastatin-NP at 3000 μg also had no effects on indices of in-stent stenosis, but modestly but significantly decreased fibrin deposition.

Effects of Pitavastatin-NP-Eluting Stents Versus Sirolimus-Eluting Stents on Endothelial Surface Coverage

As previously reported, re-endothelialization was not impaired at sirolimus-eluting stent sites four weeks post-stenting. There was no significant difference in the re-endothelialization score among the four groups four weeks after stenting (**Table 3**); therefore, the endothelial surface coverage was examined at earlier time points (seven days post-stenting) by scanning electron microscopy. At bare metal stent sites, almost complete endothelial coverage was noted above and between stent struts at seven days (**Fig. 7**). Similar magnitudes of endothelial coverage were observed at FITC-NP-eluting stent and pitavastatin-NP-eluting stent sites. In contrast, endothelial coverage was impaired at sirolimus-eluting stent sites; regions lacking endothelial coverage were generally associated with platelet aggregation and adherent leukocytes.

Serum and Tissue Concentrations of Pitavastatin

Tissue concentrations of pitavastatin were below the limit of detection (2.5 ng/g protein) in coronary artery segments three hours after the deployment of pitavastatin-NP-eluting stents. In addition, serum levels of pitavastatin were below the limit of detection (1 ng/mL) one and three hours after the deployment of pitavastatin-NP-eluting stents.

Discussion

We here report the first successful development of pitavastatin-NP-eluting stents with a newly invented cationic electrodeposition coating technology. We previously showed that (1) PLGA-NP was taken up actively by VSMC and endothelial cells mainly via endocytosis and was retained stably in the intracellular space and that (2) NPs may slowly release encapsulated drugs as PLGA is hydrolyzed[22, 23] This bioabsorbable polymeric NP-eluting stent system has unique aspects with respect to vascular compatibility and efficient drug delivery (stable delivery of NPs into the neointima and medial layers until day 28 after deployment of the NP-eluting stent), as compared to dip-coated polymer-eluting stents[22]. Importantly, this NP drug delivery system can carry hydrophilic agents such as statins, which offer advantages over the current stent-coating technology. In addition, this NP-eluting stent system provided an effective means of delivering NP-incorporated drugs or genes that target intracellular proteins involved in the pathogenesis of

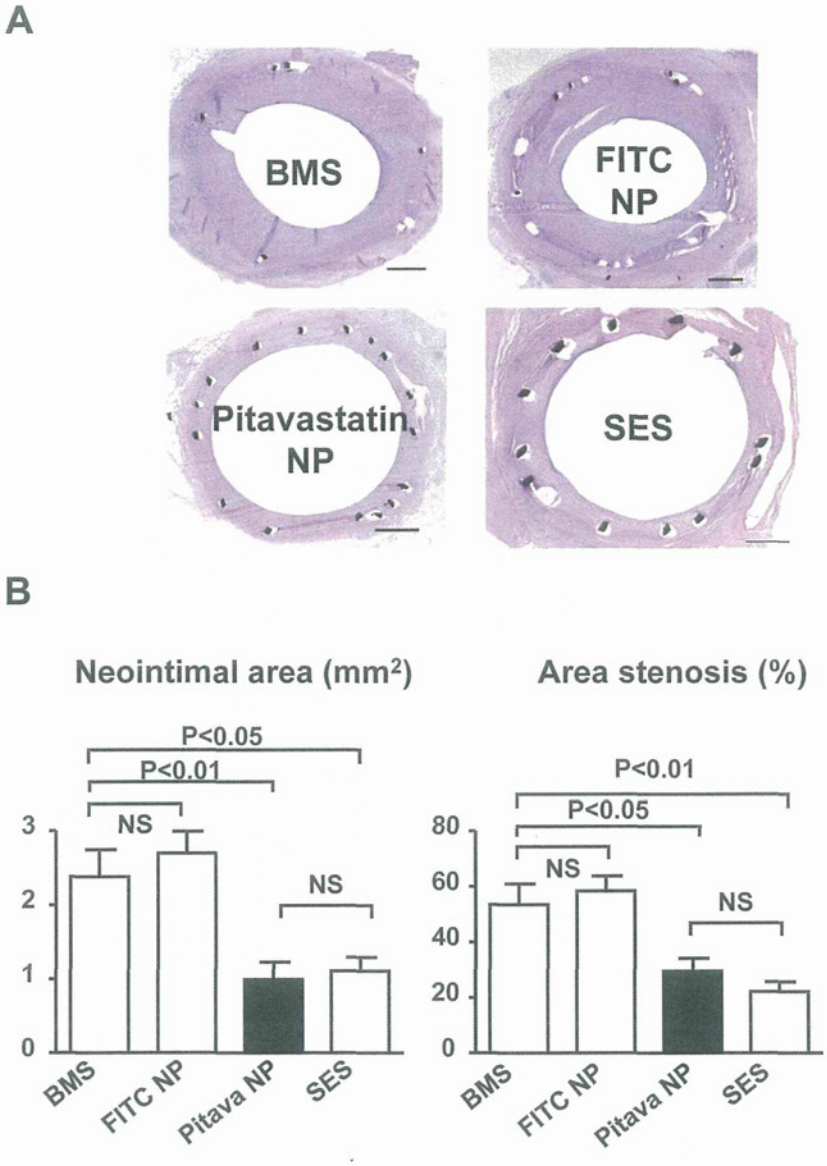

Fig. 5. Histopathological analysis of in-stent neointima formation four weeks after stent implantation.

A, Coronary artery cross-sections stained with hematoxylin-eosin from bare metal stent (BMS), FITC-NP-eluting, pitavastatin-NP-eluting, and sirolimus-eluting stent (SES) groups. Bar = 0.5 mm. B, Neointima area (mm^2) and % stenosis [100 × (area of internal elastic lamia - neointima area) / area of internal elastic lamia] in bare metal stent ($n = 10$), FITC-NP-eluting stent ($n = 12$), pitavastatin-NP-eluting stent ($n = 12$) stent, and sirolimus-eluting stent ($n = 12$) groups.

in-stent neointima formation; therefore, this NP-eluting stent system may work as an excellent platform for delivering therapeutic agents.

The pleiotropic (non-LDL-related) vasculoprotective effects of statins are mediated through reduced levels of cholesterol biosynthesis intermediates that serve as lipid attachments for posttranslational modifications (isoprenylation) of proteins, including Rho and Rac[8]. In the present study, pitavastatin was selected as the nanoparticulation compound because this compound elicited (1) the most potent inhibitory effects on human VSMC proliferation (**Table 1**), and (2) the greatest effects on the re-endothelialization response of human endothelial cells and on the inhibition of tis-

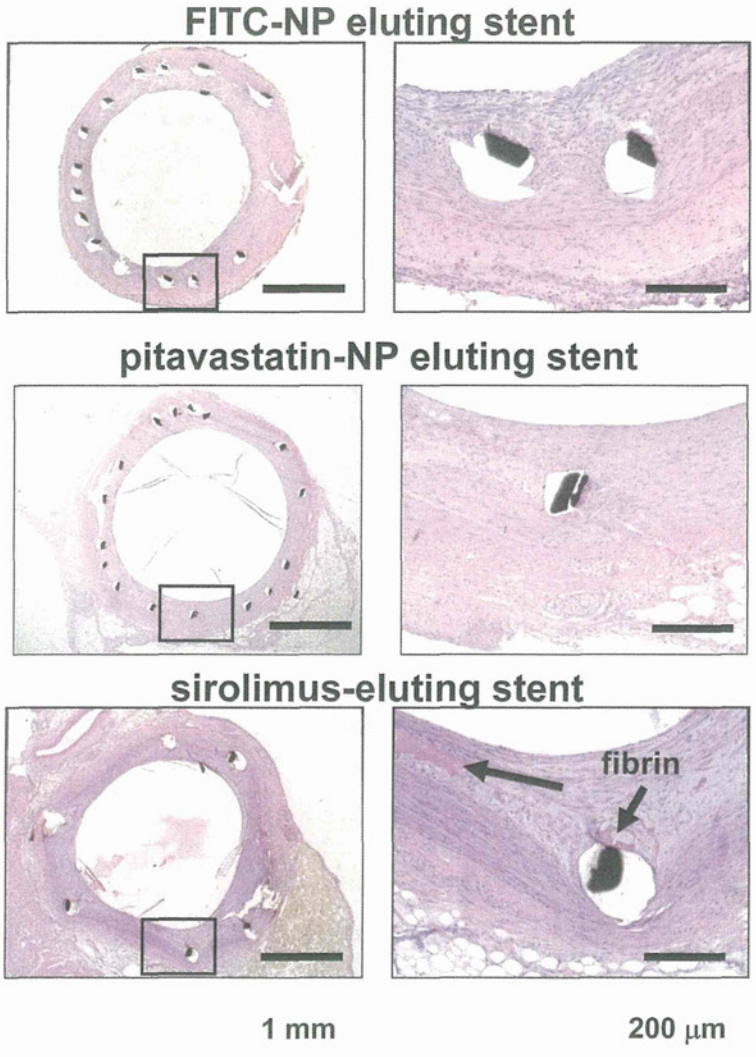

Fig. 6. Representative low- (left panels) and high-magnification (right panels) micrographs of coronary artery cross-sections stained with hematoxylin-eosin after four weeks from FITC-NP-eluting, pitavastatin-NP-eluting, and sirolimus-eluting stent groups.

sue factor expression (**Fig. 1** and **2**). A possible explanation for the discrepancy in the effect of VSMC proliferation between hydrophilic and lipophilic statins is that, under *in vitro* conditions, hydrophilic statins are hardly incorporated into vascular tissues or vascular smooth muscle cells while lipophilic statins are more widely taken up by vascular tissues and cells via passive diffusion. Pitavastatin normalized sirolimus-induced inhibition of eNOS activity in human endothelial cells (**Fig. 3**). In addition, pitavastatin-NP was as effective as non-nanoparticulated pitavastatin at an approximately 100-fold lower dose for inhibition of VSMC proliferation (**Fig. 4**). Collectively, these *in vitro* data suggest that the NP-mediated delivery of pitavastatin may be more effective than pitavastatin alone in inhibiting VSMC proliferation and tissue factor expression and in promoting re-endothelialization.

We previously reported the central role of monocyte-mediated inflammation in the pathogenesis of in-stent neointima formation[28-31] and the formulation of polymeric gene-eluting stents or nuclear factor kappa-B decoy, inhibiting in-stent stenosis[28, 32]; however, although advanced polymer technology was used, we were not able to formulate appropriate statin coating on metallic stents (authors' unpublished observation). An important finding of this study is that pitavastatin-NP-eluting stents attenuated in-stent stenosis (neointima formation) as effectively as sirolimus-eluting

Table 3. Re-endothelialization, injury score, inflammation score, and fibrin score 4 weeks after stenting

	BMS ($n=10$)	FITC-NP stent ($n=12$)	Pitavastatin -NP stent ($n=12$)	SES ($n=12$)	p value
Re-endothelialization score	2.70 ± 0.15	2.83 ± 0.11	2.83 ± 0.11	2.08 ± 0.43	NS
Injury score	1.31 ± 0.03	1.39 ± 0.07	1.36 ± 0.05	1.42 ± 0.11	NS
Inflammation score	1.65 ± 0.14	1.64 ± 0.07	1.08 ± 0.14*	2.38 ± 0.12**	$p<0.0001$
Fibrin score	0.30 ± 0.15	0.58 ± 0.19	0.65 ± 0.18	2.00 ± 0.21**	$p<0.0001$

Data are the mean ± SEM. *$p<0.05$, **$p<0.01$ versus control bare metal stent by Kruskal-Wallis test followed with non-parametric Dunn's multiple comparison tests. NS: Not Significant.

The re-endothelialization score was defined as the extent of the circumference of the arterial lumen covered by endothelial cells and was scored from 1 to 3 (1=25%; 2=25% to 75%; 3=>75%).

The injury score was determined at each strut site, and mean values were calculated for each stented segment. In brief, a numeric value from 0 (no injury) to 3 (most injury) was assigned: 0=endothelial denudate, internal elastica lamina (IEL) intact; 1=IEL lacerated, media compressed, not lacerated; 2=IEL lacerated, media lacerated, external elastica lamina (EEL) compressed, not lacerated; and 3=media severely lacerated, EEL lacerated, adventitial may contain stent strut. The average injury score for each segment was calculated by dividing the sum of injury scores by the total number of struts in the examined section.

The inflammation score took into consideration the extent and density of the inflammatory infiltrate in each individual strut. With regard to the inflammatory score for each individual strut, the grading is: 0=no inflammatory cells surrounding the strut; 1=light, non-circumferential inflammatory cell infiltrate surrounding the strut; 2=localized, moderate to dense cellular aggregate surrounding the strut non-circumferentially; and 3=circumferential dense inflammatory cell infiltration of the strut. The inflammatory score for each cross section was calculated in the same manner as for the injury score (sum of the individual inflammatory scores, divided by the number of struts in the examined section).

The intimal fibrin content was graded as 0, no residual fibrin; 1, focal regions of residual fibrin involving any portion of the artery or moderate fibrin deposition adjacent to the strut involving <25% of the circumference of the artery; 2, moderate fibrin involving >25% of the circumference of the artery or heavy deposition involving <25% of the circumference of the artery; or 3, heavy fibrin deposition involving >25% of the circumference of the artery.

Table 4. Effects of intracoronary saline or Pitava-NP on histopathological morphometry and scoring 4 weeks after stenting

	saline ($n=5$)	Pitavastatin-NP 300 μg ($n=6$)	Pitavastatin-NP 3000 μg ($n=6$)	p value
Morphometry at stent sites				
Lumen area	2.88 ± 0.25	2.29 ± 1.01	2.72 ± 0.88	NS
Media area	0.95 ± 0.12	1.25 ± 0.32	0.92 ± 0.13	NS
Neointimal area	1.80 ± 0.14	2.30 ± 0.93	1.92 ± 0.88	NS
Scores at stent sites				
Injury score	1.00 ± 0.0	1.22 ± 0.13	1.04 ± 0.05	NS
Inflammation score	1.33 ± 0.0	1.47 ± 0.46	1.23 ± 0.08	NS
Fibrin score	0.75 ± 0.09	0.74 ± 0.27	0.39 ± 0.16*	$p<0.05$
Endothelization score	2.00 ± 0.0	1.80 ± 0.27	1.98 ± 0.03	NS

Data are the mean ± SEM. *$p<0.05$ versus control bare metal stent by Kruskal-Wallis test followed with non-parametric Dunn's multiple comparison tests. NS: not significant.

stents in a porcine coronary artery model. It is likely that local mechanisms are involved in the mechanism of the therapeutic effects of pitavastatin-NP eluting stents, because intracoronary administration of pitavastatin-NP at 300 μg (an equivalent dose to that coated on pitavastatin-NP-eluting stent) showed no effects. A prior study reported that oral administration of pitavastatin at 40 mg/body per day for five weeks inhibited in-stent stenosis in a porcine coronary artery model[12]. The estimated dose of pitavastatin loaded on our NP-eluting stent was 20 ± 4 μg/stent, which is much lower than the cumulative systemic dose used in a prior study (40 × 35 days = 1350 mg/body)[12]. We measured the local tissue concentrations of pitavastatin with HPLC and found them to be under the limit of detection immediately after the deployment of the pitavastatin-NP-eluting stent; therefore, the local concentration of pitavastatin after deployment of the pitavastatin-NP-eluting stent is unclear, but is less than the limit of detection (2.5 ng/g protein or 1 ng/mL).

Delayed endothelial healing effects characterized